ACS Partner Journal

CHEM & BIO ENGINEERING

pubs.acs.org/ChemBioEng

Article

Effect of W Modification on MoS_2 Surface Edge in the Ethanolysis of Lignin into Platform Chemicals

Kai Wu, Qian Zhang, Yuanbo Zheng, Jun Yuan, Qinwei Yu, Jianming Yang,* and Jian Lu

Cite This: *Chem Bio Eng.* 2024, 1, 725−736

Read Online

ACCESS | Metrics & More | Article Recommendations | Supporting Information

ABSTRACT: A series of metal-doped MoS_2, including W-, V-, and Re-doped MoS_2, are prepared via a two-step hydrothermal method, which presents higher activity on the depolymerization of enzymatic hydrolysis lignin (EHL) in ethanol as compared to undoped MoS_2. At 320 °C for 6 h, the highest overall aromatic monomer yield of 231 mg/g EHL, including alkylphenols (A-Ps) as the main products with a yield of 126.5 mg/g EHL, is obtained over two-step hydrothermally prepared W-doped MoS_2 with the W/Mo molar ratio of 0.1 (Ts-$W_{0.1}$@MoS_2). The W-doped MoS_2 sample gives higher enhancement of EHL bio-oils' heating value to 37.1 MJ/kg as compared to Re and V modified MoS_2. Large distribution of W atoms on the MoS_2 surface in two-step hydrothermally synthesized samples leads to the higher activity of EHL depolymerization than one-step prepared samples. The reduction of W precursors on the MoS_2 surface in the preparation process promotes the generation of more Mo^{5+} and Mo^{6+}, which plays important roles in the improvement of EHL depolymerization activity. The effect of the W-doping modification and the stability of W-doped MoS_2 are discussed. The anti-sulfur loss and antioxidant abilities are significantly enhanced after W-doping modification. In the recyclability test, the good incorporation of W atoms with MoS_2 surface and the gradual oxidation of W-based sites improve the balance of catalytic cycles among different Mo-based sites, which results in the increase of catalyst stability.

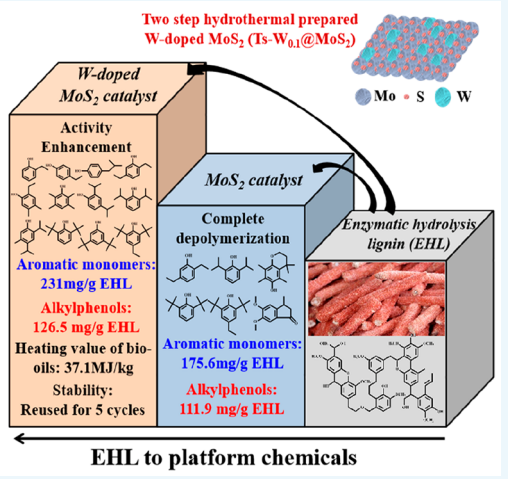

KEYWORDS: *W modification, MoS_2 surface edge, two-step hydrothermal method, lignin ethanolysis, aromatic monomers*

1. INTRODUCTION

Nowadays, the crisis of increasing depletion of fossil fuels has drawn widespread concern. Wide-range research on the development of searching renewable resources has been investigated.[1] Lignocellulosic biomass was regarded as one of the most potential materials to produce chemicals and fuels in consideration of its abundant and cheap properties.[2,3] Lignin, which was the only natural macromolecule polymer enriched with benzene ring structures, was the most recalcitrant components and accounts the weight percentage of ∼35 wt % in lignocellulosic biomass.[4−6] Extensive research on lignin conversion strategies has been explored in recent decades.[7−10] Normally, pyrolysis bio-oils would be the main downstream products in a commercialized biorefinery process. Nevertheless, bio-oils exhibited poor properties of high oxygen content, molecular complexity, or corrosiveness, which limited their further commercial application.[11−13] Hence, developing an efficient technological process for the simultaneous achievement of lignin depolymerization and deoxygenation of lignin-derived bio-oils into high value-added chemicals becomes a more attractive and urgent issue.

Recently, MoS_2 had been considered as one of the optimal candidates with high performance in the hydrogen evolution reaction (HER).[14,15] Meanwhile, the enhancement investigation of MoS_2 activity by metal-doping method (Co or Ni) had been widely extended to bring out its greater value in the biorefinery process such as hydrodeoxygenation (HDO) of pyrolysis bio-oils.[16−19] From these early HDO academic studies, Shabtai et al.[16] prepared a series of γ-Al_2O_3-supported transition metal-containing catalysts to examine the performance on hydrogenolysis of C−O linkage in diphenyl ether, where Co, Ru, and Rh were proved to be the best promoters. Bui et al. observed that the HDO of guaiacol-type molecules on the MoS_2-based catalyst is greatly improved with the promoting of cobalt.[18]

Generally, the improved activity of the catalyst by inserting Co or Ni atoms on MoS_2 edge was contributed to significant change in texture and structure properties, which led to the acceleration of proton adsorption and heteroatoms' activation

Received: October 11, 2023
Revised: January 4, 2024
Accepted: January 4, 2024
Published: January 31, 2024

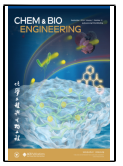

https://doi.org/10.1021/cbe.3c00062
Chem Bio Eng. 2024, 1, 725−736

(i.e., S, N, or O atoms).[20,21] Metal nitrates are commonly employed as the precursors in the metal-doping process. Nevertheless, sulfide phases of doping metal would be easily generated, which might be due to the large difference in precipitation rate for doping metal and sulfur ions. The interaction of modified atoms with MoS_2 could persecute the surface engineering of MoS_2 to release higher catalytic activity.[22,23] Hydrothermal methods that tuned the composition of surface atoms with diverse solvents and precursors were attractively investigated by many researchers and were regarded as an efficient strategy for improvement of MoS_2 surface edge structure and active sites. Shi et al.[24] reported a strategy to improve the HER activity of MoS_2 by engineering its energy level via a direct metal doping through a hydrothermal process with *N*,*N*-dimethylformamide as solvent. The superior electrochemical performance of Zn-doped MoS_2 was found to far exceed MoS_2. Wu et al.[25] prepared a porous and defect-rich CoMoS nanomaterial to improve the HER performance via a solvothermal treatment with ammonium molybdate and cobalt nitrite as precursors. A two-step hydrothermally prepared CoS_2/MoS_2 was performed for HDO of phenols, which minimized hydrogen consumption and exhibited higher deoxygenation activity than MoS_2.[26] Subsequently, Song et al.[27] proposed a self-introduced method by co-substituted S sites on the MoS_2 nanosheets by a two-step hydrothermal method. This strategy achieved significant promotion of HDO activity for lignin-derived phenolics. Diphenyl ether was almost completely converted into arene (including 98% of benzene and 2% of phenol) over CoMoS at 300 °C under 4.0 MPa H_2.

Commonly, loss of sulfur atoms on MoS_2 would easily prompt the deactivation of the catalyst.[28] Therefore, the metal-doping methodology provides a novel strategy to stabilize the surface atoms on MoS_2 through the formation of certain stable phases (i.e., Co−Mo−S phase). Nevertheless, most research about the modification of the MoS_2 surface by the metal-doping method was focused on the HDO process of lignin-derived bio-oils. To the best of our knowledge, the effect of metal doping on the biomass conversion (especially lignin depolymerization in low-carbon alcohols) has not been reported so far. Moreover, except for traditionally applied Co and Ni metals, elements in the same VIB family (W, etc.) or diagonal (V or Re) with molybdenum in the periodic table of elements were never reported on MoS_2 surface modification. The similar properties among these sulfides with MoS_2 are likely to provide efficient solutions to improve the activity and stability of MoS_2 on enzymatic hydrolysis lignin (EHL) ethanolysis.

In this work, a series of active metal-doped (i.e., metals Re, V, W, Fe, Co, and Ni) MoS_2 samples were prepared via a two-step hydrothermal method, which were tested for ethanolysis of EHL. The doped MoS_2 samples were characterized by X-ray photoelectron spectroscopy (XPS), scanning transmission electron microscopy-energy-dispersive X-ray (STEM-EDX) spectroscopy, and X-ray fluorescence (XRF) spectroscopy to reveal the effect of dopant on the active sites on the MoS_2 surface. To compare the advantages of two-step hydrothermal methods, the activity of one-step hydrothermally synthesized W-doped MoS_2 was also investigated. The mechanism of improved stability for W-doped MoS_2 was also examined.

2. EXPERIMENTAL SECTION

2.1. Materials. Enzymatic hydrolysis lignin (EHL) was obtained from Shandong Longlive Biotechnology Co., Ltd. The EHL sample is dried at 60 °C overnight before use. The solvents and chemicals such as ethanol, ethyl acetate, thioacetamide, sodium molybdate, ammonium metatungstate, ammonium vanadate, ammonium perrhenate, cobalt nitrate, nickel nitrate, iron nitrate, anisole with analytical reagent grade, hydrazine hydrate solvents (85%), and concentrated hydrochloric acid (∼37%) were purchased from Tianjin Guangfu Technology Development Co., Ltd. Deionized water was prepared with an ultrapure water purification machine (UPH-1-10).

2.2. Catalyst Preparation. Molybdenum sulfide was prepared with a one-pot hydrothermal method referring to our previous work.[29] In brief, Na_2MoO_4 and CH_3CSNH_2 were used as the Mo and S precursors, respectively. The hydrothermal reaction was operated at 200 °C for 24 h.

I. Two-step hydrothermal method for preparation of X-doped MoS_2 (X = Re, V, W, Fe, Co, and Ni). The first step is to prepare the MoS_2 catalyst as mentioned above. In the second step, the precursors of active metals (i.e., ammonium of perrhenate (NH_4ReO_4), vanadate (NH_4VO_3), and metatunstate ($(NH_4)_6H_2W_{12}O_{40}\cdot xH_2O$) and nitrate of cobalt ($Co(NO)_2\cdot 6H_2O$), nickel ($Ni(NO_3)_2\cdot 6H_2O$), and iron ($Fe(NO_3)_3\cdot 9H_2O$)) are dissolved in 29 mL of water to obtain a solution with the expected molar ratio of X/Mo. 0.3 g of prepared MoS_2 and ∼1 mL of hydrazine hydrate are subsequently added into the solution to form a slurry, which was then ultrasonicated for 30 min. Afterward, the slurry is transferred into the 50 mL reactor and maintained at 200 °C for 24 h. The obtained catalyst with the molar ratio of X/Mo = 0.5 is named as Ts-$X_{0.5}$@MoS_2 ("Ts" means two-step hydrothermal method). Similarly, the W-doped MoS_2 with different molar ratios of W to Mo (x) is named as Ts-W_x@MoS_2 (x = 0.5, 0.25, 0.167, 0.125, and 0.1).

II. One-step hydrothermal method for preparation of W-doped MoS_2. In a typical run, a certain amount of $(NH_4)_6H_2W_{12}O_{40}\cdot xH_2O$, ∼6 g of Na_2MoO_4, and ∼9.4 g of CH_3CSNH_2 were initially dissolved in a mixed solvent of 15 mL of deionized water and 15 mL of ethanol. Meanwhile, ∼3 mL of concentrated hydrochloric acid was added to the solution, which was further ultrasonicated and stirred for 30 min to form a slurry and then transformed into a 50 mL stainless-steel reactor for hydrothermal reaction at 200 °C for 24 h. The obtained sample with different molar ratio of W to Mo (x) was named as Os-W_x@MoS_2 (x = 0.5, 0.25, 0.167, 0.125, and 0.1, "Os" mean one-step hydrothermal method).

After the preparation of different samples, the precipitate was obtained through vacuum filtration and subsequently washed with 50/50 vol of ethanol/deionized water three times. Finally, the solid was dried in a vacuum oven at 60 °C overnight prior to characterization and use.

2.3. Catalyst Characterization. N_2 adsorption−desorption analysis is used to obtain the texture data of samples, and the measurement was operated with a Quantachrome Autosorb-1 equipment at liquid nitrogen temperature (−196 °C). X-ray diffraction (XRD) patterns of fresh and used catalysts were recorded at room temperature by using a Bruker D8 Advance instrument with Cu Kα radiation, which was operated at 40 kV and 40 mA at a scanning rate of 10°/min in the 2θ range of 10−90°. The scanning transmission electron microscope (STEM) images were taken with a JEM-2100F (JEOL) instrument with an acceleration voltage of 200 kV. The energy dispersive X-ray (EDX) analysis was performed on a Genesis XM2 instrument to observe the dispersion of W atoms on the MoS_2 surface. X-ray photoelectron spectroscopy (XPS) for fresh and used samples was applied to trace the change of surface states. The measurements were taken with a PHI 1600 ESCA system spectrometer equipped with Mg Kα X-ray source (1253.6 eV). After charging by the C 1s peak (284.6 eV), the corresponding spectra were fitted by a combination of Gaussian and Lorentzian functions with the CasaXPS and Avantage softwares. X-ray fluorescence (XRF) spectroscopy was performed on a Axios (Panalytical) instrument under the operation voltage of 60 kV and current of 50 mA.

https://doi.org/10.1021/cbe.3c00062
Chem Bio Eng. 2024, 1, 725−736

Inductively coupled plasma emission spectrometry (ICP) was measured with an Optima 5300DV instrument (Perkin Elmer).

2.4. Catalytic Reactions. The EHL depolymerization reaction was carried out in a 300 mL batch reactor (made of Hastelloy, from Huotong Co., Anhui province). In a typical run, 0.2 g of EHL, 70 mL of ethanol, and 0.1 g of the catalyst were loaded into the autoclave reactor. The reactor was sealed and purged with pure nitrogen several times and then heated to the desired temperature at a heating rate of 3 °C/min with the stirring rate of 600 rpm. While the reaction was finished, the reactor was immersed in a cold-water bath and cooled rapidly to room temperature. The gas was released followed by the separation of solid residue from liquid products by suction filtration. The used catalyst was dried at 60 °C in a vacuum overnight for further characterization and recyclability test. The post-reaction liquids obtained from EHL depolymerization were evaporated in a vacuum rotary evaporator at 35 °C to remove ethanol for further quantitative and qualitative analysis.

2.5. Product Analysis. All of the liquid products were quantified using veratrole as an internal standard, which was performed with a gas chromatograph equipped with a flame ionization detector (GC-FID, Agilent Technologies, model 6890) and a HP-5 MS capillary column (Agilent, 30 m × 0.25 mm × 0.25 μm). The GC parameters are injector temperature 280 °C, detector temperature 300 °C, and split ratio 1:50. The temperature is increased to 250 °C at 10 °C/min after holding for 2 min at 100 °C, and then it is kept for 5 min. The qualitative analysis of products is detected with a mass selective detector (MSD, Agilent Technologies, model 5973) with the aid of the library of the National Institute of Standards and Technology (NIST). The yield of overall aromatic monomers and alkylphenols (A-Ps) were calculated according to eqs 1. In the equation, m represents the mass of each corresponding chemical. The calculated value is confirmed by the average of the data measured three times. The heating values of the bio-oils was estimated by the Dulong formula of eqs 2, where X_C, X_H, and X_O represent the weight percentage of carbon, hydrogen, and oxygen in the samples, respectively.

$$\text{Yield (mg/g EHL)} = \frac{m(\text{overall aromatic monomers or A-Ps})_{\text{output}}}{m(\text{EHL})_{\text{input}}} \quad (1)$$

$$\text{Heating value (MJ/kg)} = 33.8X_C + 142.8(X_H - 0.125X_O) \quad (2)$$

The two-dimensional heteronuclear single quantum coherence-nuclear magnetic resonance (2D-HSQC NMR) spectra were detected on a Bruker AVAVCE III HD at 400 MHz. The deuterium generation reagent was DMSO-d_6.

3. RESULTS AND DISCUSSION

3.1. Catalyst Characterization. Figure 1 presents the XRD patterns of fresh Ts-$X_{0.5}$@MoS_2 (X = Fe, Ni, Co, Re and V) and Os-$W_{0.125}$@MoS_2 samples and of Ts-$W_{0.1}$@MoS_2 (fresh and used after 5 runs). For the fresh Ts-$Fe_{0.5}$@MoS_2 and Ts-$Ni_{0.5}$@MoS_2, the diffraction peaks of orthorhombic FeS_2 (PDF#37-0475) and cubic NiS_2 (PDF#11-0099) phases are observed, respectively. The peak of the cubic Co_3S_4 phase at 31.2°, 38.3°, 49.8°, and 57.4° (PDF#42-1448) is observed in the fresh Ts-$Co_{0.5}$@MoS_2 sample. Nevertheless, the signals assigned to MoS_2 are not detected, which indicates that the MoS_2 phase was badly damaged when metal nitrates are used as doping precursors. Nevertheless, for the fresh V-, Re-, and W-doped MoS_2 samples, only the diffraction peaks at 14.5°, 33°, and 58.3° indexed to the (003), (101), and (110) planes, respectively, for the hexagonal MoS_2 phase (PDF#17-0744) are observed, which resembled the XRD patterns of pure HT-MoS_2 reported in our previous work.[29] The results reveal that the V, Re, and W sulfide phases are not formed in their

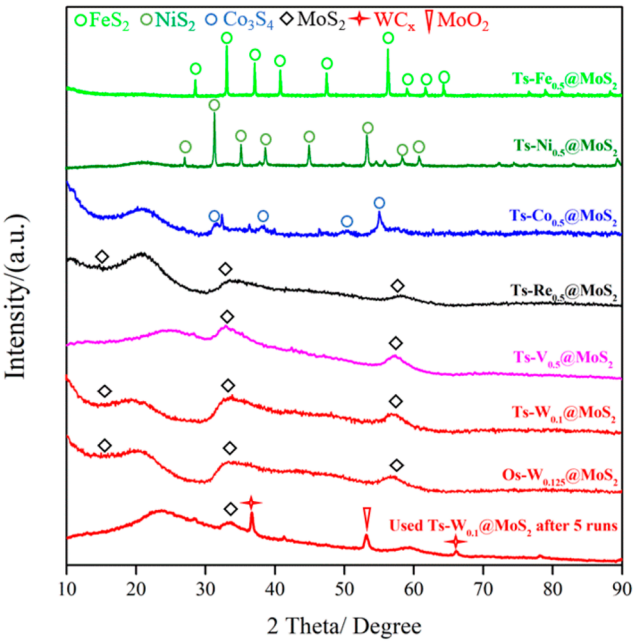

Figure 1. XRD patterns of fresh Ts-$Fe_{0.5}$, $Co_{0.5}$, $Ni_{0.5}$, $Re_{0.5}$, $V_{0.5}$@MoS_2, and Os-$W_{0.125}$@MoS_2 samples and Ts-$W_{0.1}$@MoS_2 (fresh and used after 5 runs).

corresponding modified MoS_2 catalyst. After 5 runs use of Ts-$W_{0.1}$@MoS_2, the peak at 53.8° contributed to the (102) plane in the MoO_2 phase (PDF#50-0739) and the peaks at 22.2°, 59.7°, and 66° indexed to the (103), (513), and (228) planes, respectively, in the hexagonal MoC_x phase (PDF#20-1314) are identified.

Table 1 lists the specific texture data of fresh MoS_2, Os-$W_{0.125}$@MoS_2, and Ts-$W_{0.1}$@MoS_2 (fresh and used after 5 runs). In comparison to MoS_2, the fresh Ts-$W_{0.1}$@MoS_2 sample has a larger specific surface area (160 m^2/g), whereas Os-$W_{0.125}$@MoS_2 has smaller data (4 m^2/g). The pore volume of both Ts-$W_{0.1}$@MoS_2 (5.0 nm) and Os-$W_{0.125}$@MoS_2 (18.4 nm) samples are larger than that of MoS_2 (3.7 nm). As shown in Figure S1, the isotherms of the Ts-$W_{0.1}$@MoS_2 and Os-$W_{0.125}$@MoS_2 are confirmed with type-IV, which are consistent with the mesoporous feature of materials. After 5 runs of use, the specific surface area and pore volume of the Ts-$W_{0.1}$@MoS_2 sample were decreased into 13 and 0.04 cm^3/g, respectively. Nevertheless, the pore diameter was increased largely into 15.8 nm.

Table 1. Texture Data of MoS_2, Ts-$W_{0.1}$@MoS_2, Os-$W_{0.125}$@MoS_2, and Used Ts-$W_{0.1}$@MoS_2 after 5 Runs

Entry	Catalyst	Specific surface area (m^2/g)	Pore volume (cm^3/g)	Pore diameter (nm)
1	MoS_2	108	0.47	3.7
2	Ts-$W_{0.1}$@MoS_2	160	0.26	5.0
3	Os-$W_{0.125}$@MoS_2	4	0.02	18.4
4	Ts-$W_{0.1}$@MoS_2[a]	13	0.04	15.8

[a]Used after 5 runs.

To better understand the structure and distribution of W atoms on the surface of the Ts-$W_{0.1}$@MoS_2 sample, STEM and energy-dispersive X-ray spectroscopic mapping are further carried out, as shown in Figure 2. The Ts-$W_{0.1}$@MoS_2 sample

https://doi.org/10.1021/cbe.3c00062
Chem Bio Eng. 2024, 1, 725−736

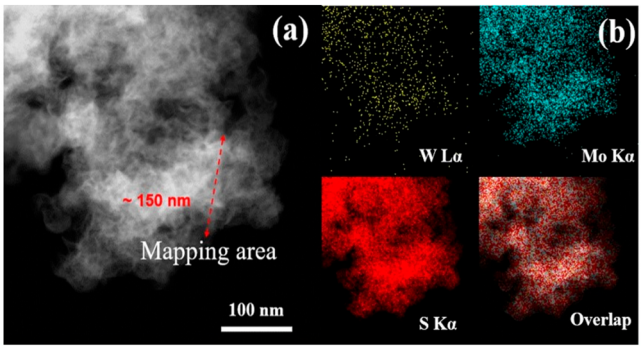

Figure 2. Electron microscopic images of as-prepared Ts-$W_{0.1}$@MoS_2 sample: (a) STEM image of nanoflowers and (b) STEM-EDX (energy-dispersive X-ray spectroscopic) mapping images indexing W Lα, Mo Kα, and S Kα intensities.

retains the same flowerlike nanosheet structure as MoS_2 with an average particle size of ~150 nm (Figure 2(a)).[29] Element mapping images indexing W, Mo, and S intensities in the specified area for the Ts-$W_{0.1}$@MoS_2 sample are shown in Figure 2(b). Obviously, tungsten atoms are homogeneously distributed on the surface of MoS_2, which reveals good incorporation of tungsten into MoS_2 nanosheet structure.

The XPS spectra of different types of modified MoS_2 samples are illustrated in Figure 3. Figure 3(a) presents the Mo 3d levels (~228−237 eV) and broad S 2s signals (~227 eV).[30−34] The XPS of Mo 3d signals of all tested samples can be divided into Mo^{4+}, Mo^{5+}, and Mo^{6+}, which individually contain two orbits of $3d_{3/2}$ and $3d_{5/2}$. Ts-$W_{0.5}$@MoS_2 contains the larger content of Mo^{5+} (24.7%), which is followed by Ts-$Co_{0.5}$@ (22.5%), $Re_{0.5}$@ (19.9%), and $V_{0.5}$@MoS_2 (17.2%). Ts-$W_{0.1}$@MoS_2 with a lower doping amount of W exhibits a higher content of Mo^{5+} (32.1%) than Ts-$W_{0.5}$@MoS_2. The contents of Mo^{4+} on all the freshly modified samples is in the range ~50−65% Figure 3(b) depicts the XPS of S 2p (~160−173 eV) signals of different samples, which are divided into S^{2-} ($2p_{1/2}$ and $2p_{3/2}$), S_2^{2-} ($2p_{1/2}$ and $2p_{3/2}$), and SO_x.[32,34] The order of the S_2^{2-} content for two-step hydrothermally synthesized samples is as follows: Ts-$Co_{0.5}$ (32.3%) > $W_{0.5}$@

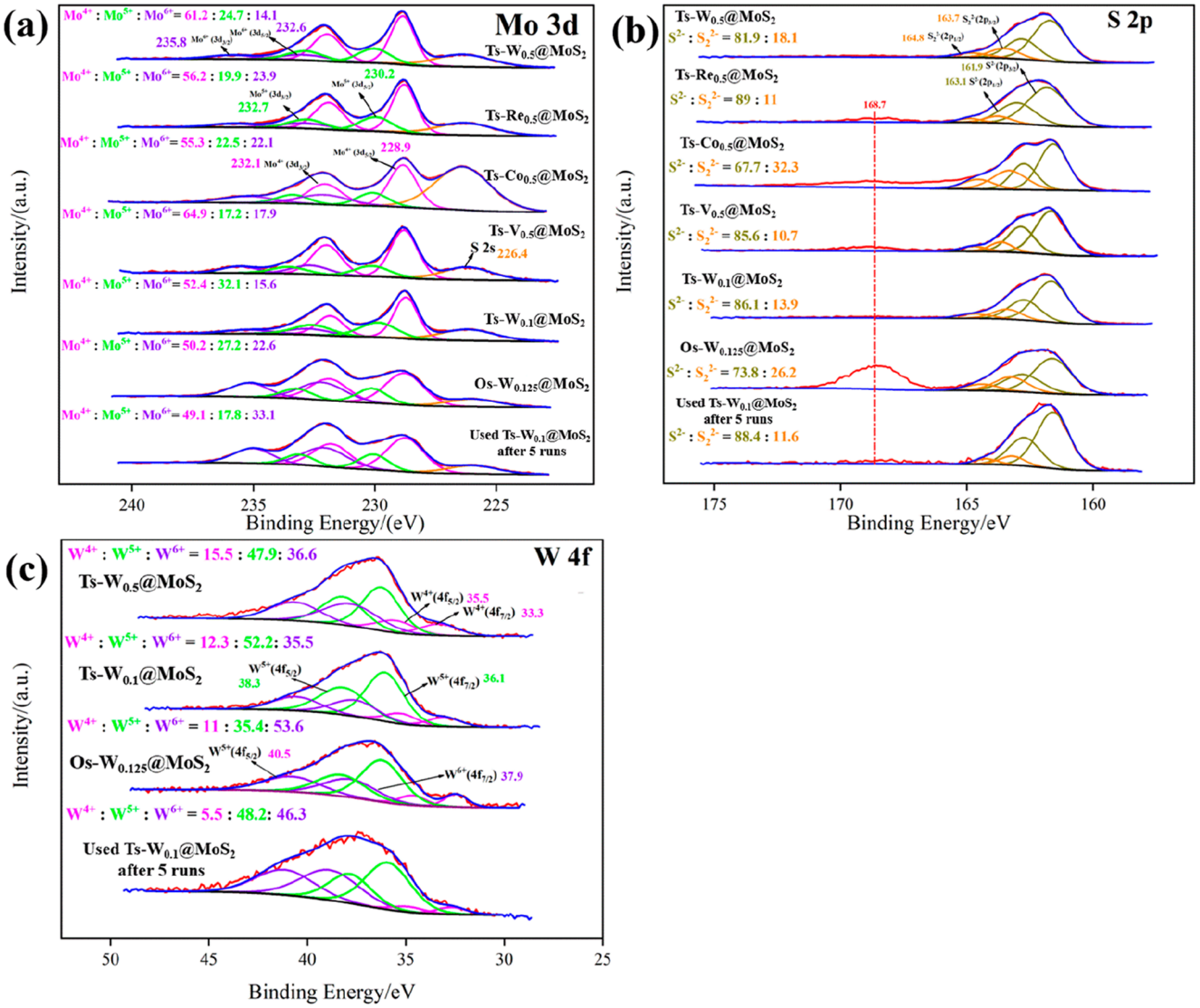

Figure 3. XPS spectra of (a) Mo 3d and (b) S 2p of active metal-doped MoS_2 catalysts and (c) W 4f of W-doped MoS_2 samples.

https://doi.org/10.1021/cbe.3c00062
Chem Bio Eng. 2024, 1, 725−736

(18.1%) >$W_{0.1}$@ (13.9%) > $Re_{0.5}$@ (11%) > $V_{0.5}$@MoS_2 (10.7%). One-step synthesized Os-$W_{0.125}$@MoS_2 contains the largest content of S_2^{2-} (26.2%) among all the prepared W-doped samples. Figure 3(c) presents the XPS of W 4f (~30−45 eV) signals of different W-doped samples, which can be assigned into W^{4+} ($4f_{5/2}$ and $4f_{7/2}$), W^{5+} ($4f_{5/2}$ and $4f_{7/2}$), and W^{6+} ($4f_{5/2}$ and $4f_{7/2}$).[35−37] The contents of W^{4+} and W^{5+} on two-step synthesized samples are in the narrow ranges 12−16% and 47−53%, respectively, which are larger than those of Os-$W_{0.125}$@MoS_2 (11% and 35.4%, respectively). Nevertheless, Os-$W_{0.125}$@MoS_2 contains much higher contents of W^{6+} (53.6%) than the two-step prepared samples, which indicates that the one-step hydrothermal method could easily lead to higher formation of WO_x. After 5 runs, the contents of Mo^{4+}, Mo^{5+}, S_2^{2-}, and W^{5+} on Ts-$W_{0.1}$@MoS_2 are decreased into 49.1%, 17.8%, 11.6%, and 48.2%, respectively (Figure 3(a−c)). In addition, the XPS of Re 4f, Co 2p, and V 2p signals of Ts-$Re_{0.5}$@MoS_2, $Co_{0.5}$@MoS_2, and $V_{0.5}$@MoS_2, respectively, are illustrated in Figure S2.

3.2. Activity Test. *3.2.1. Plausible Products in Catalytic Depolymerization of EHL.* The total-ion chromatogram (TIC) of the liquid products produced from the depolymerization of EHL over Ts-$W_{0.1}$@MoS_2 in ethanol at 320 °C and their corresponding structures are illustrated in Figure 4. Twenty-six

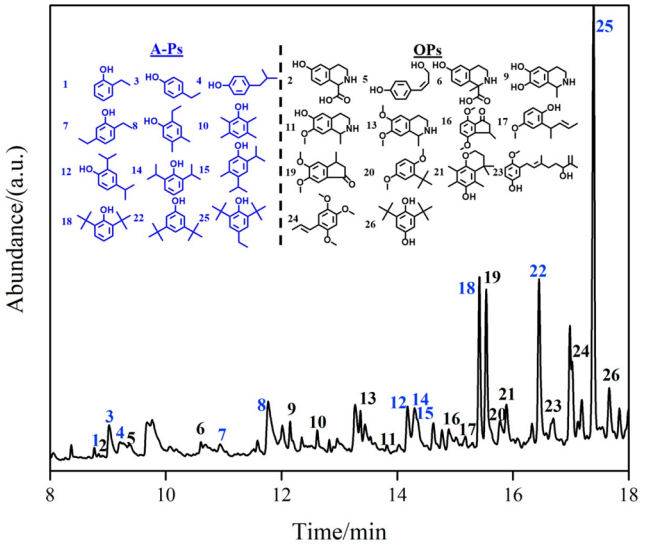

Figure 4. Total-ion chromatogram (TIC) of the liquid products obtained from EHL depolymerization and the structural distribution of the corresponding product at 320 °C for 6 h in ethanol over the Ts-$W_{0.1}$@MoS_2 catalyst.

aromatic monomers were quantified, which can be classified as two groups: alkylphenols (A-Ps) and other products (OPs). As the main products, A-Ps mainly contain di(*tert*-butyl)phenol (Nos. 18 and 22) and 2,6-di(*tert*-butyl)-4-ethylphenol (No. 25). OPs are mainly composed of 2,3-dihydro-5,6-dimethoxy-3-methyl-1*H*-inden-1-one (No. 19) and 2,6-di(*tert*-butyl)-hydroquinone (No. 26). Complete liquification of EHL without formation of char and tar was observed, and no dimers or oligomers were identified in the post-reaction products. The absence of cyclohexanol and its derivatives in the products indicates that the hydrogenation of lignin-derived aromatic monomers did not occur.

3.2.2. Activities of Different Metal-Doped MoS_2. A series of transition metals (Fe, Co, Ni, V, Re, and W) was used for modification of MoS_2 via a two-step hydrothermal method, which were then tested on the EHL depolymerization in ethanol at 320 °C. As shown in Figure 5, Ts-$Fe_{0.5}$@MoS_2 and

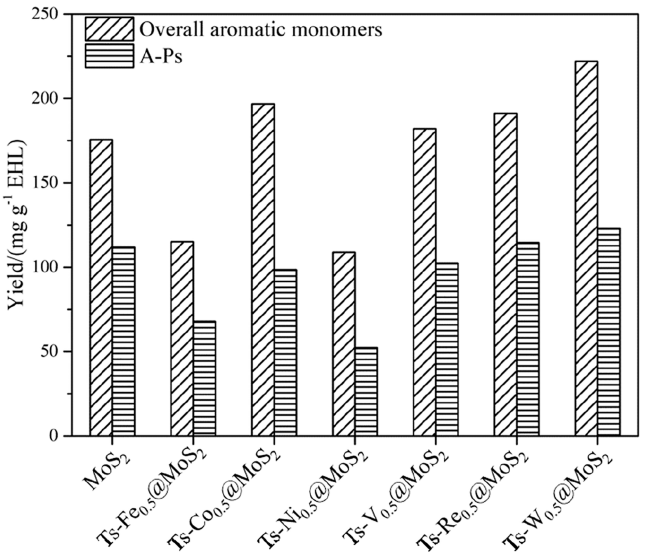

Figure 5. Yields of overall aromatic monomers and alkylphenols (A-Ps) from EHL depolymerization in ethanol at 320 °C for 6 h over Ts-$M_{0.5}$@MoS_2 (M = Fe, Co, Ni, V, W, and Re) catalysts prepared via a two-step hydrothermal method.

Ts-$Ni_{0.5}$@MoS_2 gave the lower overall aromatic monomer yield of 115.1 and 109 mg/g EHL, respectively, than that of MoS_2 (175.6 mg/g EHL). The highest overall aromatic monomer yield was obtained over Ts-$W_{0.5}$@MoS_2 (222 mg/g EHL), followed by Ts-$Co_{0.5}$@MoS_2, Ts-$Re_{0.5}$@MoS_2, and Ts-$V_{0.5}$@MoS_2 with the corresponding yield of 196.8, 191.2, and 182 mg/g EHL, respectively. The decreasing order of the A-Ps yield for different types of samples is as follows: Ts-$W_{0.5}$@MoS_2 (123.1 mg/g EHL) > Ts-$Re_{0.5}$@MoS_2 (114.6 mg/g EHL) > MoS_2 (111.9 mg/g EHL) > Ts-$V_{0.5}$@MoS_2 (102.5 mg/g EHL) > Ts-$Co_{0.5}$@MoS_2 (98.5 mg/g EHL) > Ts-$Fe_{0.5}$@MoS_2 (67.9 mg/g EHL) > Ts-$Ni_{0.5}$@MoS_2 (52.4 mg/g EHL). Obviously, tungsten is considered as the optimal doping metal on MoS_2 for the achievement of aromatic monomers and A-Ps with high yields from EHL depolymerization in ethanol.

3.2.3. Effect of W/Mo Molar Ratio and Synthesis Methods. Figure 6 illustrates the effect of different W/Mo molar ratios (from 0.1 to 0.5) and preparation methods (one- or two-step method) for different W-doped MoS_2 samples on the yields of overall aromatic monomers and A-Ps from EHL depolymerization at 320 °C. Compared to the one-step hydrothermal method, the two-step method shows obvious superiority, through which the prepared samples present higher activity for higher achievements of overall aromatic monomers and A-Ps than that through the one-step method with the same W/Mo molar ratio. To be specific, when the W/Mo molar ratios are 0.5 and 0.125, the similarly decreasing order of overall yield of aromatic monomers are Ts-$W_{0.5}$@MoS_2 (222 mg/g EHL) > Os-$W_{0.5}$@MoS_2 (182.8 mg/g EHL) > MoS_2 (175.6 mg/g EHL) and Ts-$W_{0.125}$@MoS_2 (200.8 mg/g EHL) > Os-$W_{0.125}$@MoS_2 (189.8 mg/g EHL) > MoS_2, respectively. Nevertheless, one-step prepared samples with the W/Mo molar ratio of 0.25,

https://doi.org/10.1021/cbe.3c00062
Chem Bio Eng. 2024, 1, 725−736

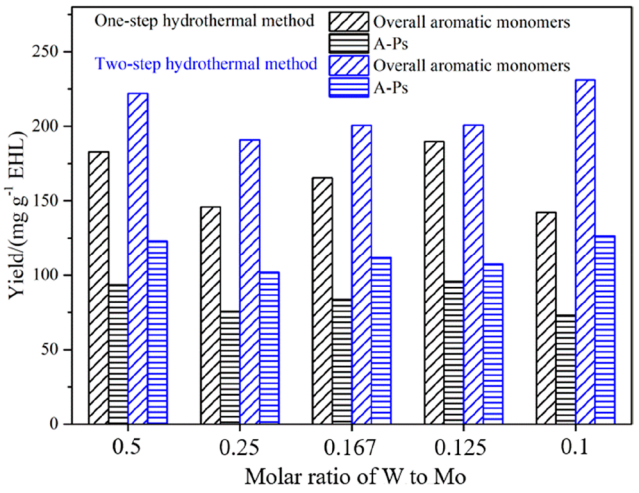

Figure 6. Yields of overall aromatic monomers and A-Ps from EHL depolymerization at 320 °C for 6 h over the W-doped MoS_2 catalyst with the W/Mo molar ratio of x (x = 0.5, 0.25, 0.167, 0.125 and 0.1) prepared via one-step and two-step hydrothermal methods.

0.167, and 0.1 gave lower activity of EHL depolymerization than that of unmodified MoS_2. The overall aromatic monomer and A-Ps yield contributed to the highest 231 and 126.5 mg/g EHL over Ts-$W_{0.1}$@MoS_2. Therefore, Ts-$W_{0.1}$@MoS_2 prepared via a two-step hydrothermal method is proved to be the optimal W-doped MoS_2 catalyst for EHL depolymerization in ethanol.

3.2.4. Heating Value of Bio-Oils. The heating values and H/C atomic ratio of bio-oils were significant parameters for the evaluation of fuels. Based on the element analysis of EHL in our previous work,[10,38] the O/C and H/C atomic ratio of EHL are 0.362 and 1.310, respectively, and the heating value of EHL was estimated as 25.0 MJ/kg calculated by the Dulong formula. When MoS_2 was used as the catalyst, the heating value and H/C atomic ratio of the post-reaction products was increased to 35.8 MJ/kg and 1.432, respectively, with the large decrease of the O/C atomic ratio from 0.362 (EHL) into 0.132 after reaction. After modified treatment of MoS_2 by doping W via a one- or two-step method, the heating value of the products was slightly increased to 36.3 or 37.1 MJ/kg, respectively. In addition, the H/C atomic ratio of the products obtained over Ts-$W_{0.1}$@MoS_2 was increased to 1.465, which was higher than that over Os-$W_{0.125}$@MoS_2 (1.406). Nevertheless, the increase of the H/C atomic ratio and complete hydrodeoxygenation of the bio-oils will be significantly needed to directly use as the jet fuel (43.2 MJ/kg).

3.3. Roles of Metal Doping on MoS_2. In most of the studies on HDO reactions, the presence of Ni or Co as a promoter in the MoS_2 catalyst was found to exhibit significant promoting effect in the improvement of HDO activity of phenolic compounds.[39] Herein, as compared with undoped MoS_2, W-, Co-, Re-, and V-doped MoS_2 catalysts all exhibit improved activity for higher production of overall aromatic monomers and A-Ps from EHL depolymerization. Based on the XRD results (Figure 1), Re, V, and W sulfide phases are not detected, which indicates that the doping metals (Re, V, and W) interact with the MoS_2 surface by atomic modification so that the MoS_2 pattern is not damaged through the two-step hydrothermal method. Nevertheless, the activities of MoS_2 with Fe and Ni as promoters are severely decreased, which may be due to the destruction of the MoS_2 structure based on XRD results (Figure 1), thus the formation of their corresponding metal phases (i.e., FeS_2 or NiS_2).

It had been well-known for a long time that only the edges (not the basal plane sites) of pure MoS_2 were active for hydrodesulfurization (HDS) and hydrodeoxygenation reactions.[40,41] The substitution of Mo at the edge of the sulfide catalyst with doped metal cations (i.e., Co and Ni) was the generally accepted explanation for understanding the mechanism of metal-doping modification of MoS_2 to improve its activity.[42,43] The doped atoms promoted the increase of the concentration of S-vacancies on the MoS_2 surface, which were regarded as the active sites for HDS. Based on our previous work, three different active phases were identified on the surface of the hydrothermally synthesized MoS_2 catalyst, namely, the MoS_2 phase (with S^{2-} species), Mo oxysulfide phase (MoO_xS_y, with S_2^{2-} species), and MoO_3 phase, which were attributed to Mo^{4+}, Mo^{5+}, and Mo^{6+} respectively.[29] In this work, three above-mentioned species still exist on the W-, Re-, and V-doped MoS_2 (Figure 3(a)), and their contents on the MoS_2 surface are significantly influenced with the effect of metal doping. In our previous study of guaiacol demethoxylation (DMO), guaiacol was converted into mainly alkylphenols over hydrothermally synthesized MoS_2 in low-carbon alcohols.[29] That indicated A-Ps obtained from EHL depolymerization are likely to be formed through the DMO process with the effect of MoS_2, in which Mo^{5+} in the MoO_xS_y phase acted as the active sites.[29,44] Herein, the doping of W, Re, and V obviously led to the decrease of Mo^{4+} (Figure 3a)), which indicated the promotion effect of active metals to convert Mo^{4+} into Mo^{5+} or Mo^{6+}. Mo^{5+} was the active site for the alkylphenol production; thus Mo^{5+}/Mo^{4+} could be a standard to evaluate the catalytic activity to produce A-Ps via the DMO process. As shown in Figure 7, the yields of A-Ps over W- and Re-doped catalysts were higher than that over MoS_2, and the Mo^{5+}/Mo^{4+} exhibited the same changing trend. However, $V_{0.5}$@MoS_2 showed the inhibition effect for A-Ps production due to the Mo^{5+}/Mo^{4+} was significantly decreased after V-doping. As for the other aromatic products, the previous work had proved that proper oxidation of Mo-based sites in suitable range could efficiently promote the EHL ethanolysis into aromatic monomers.[45] Therefore, proper conversion of Mo^{4+} into Mo^{6+} might improve the activity to obtain the other aromatic monomers, which was proved by the increased yields of the other products after all the active metals' doping as comparison to MoS_2 (Figure 7). Nevertheless, for each doped catalyst, the higher the Mo^{6+}/Mo^{4+}, the lower the activity to obtain the other products. The results implied that excessive oxidation of Mo-based sites did not benefit the achievement of aromatic monomers with high yield.

Moreover, the O/C atomic ratio of EHL depolymerized products, mainly containing A-Ps, was drastically decreased from 0.362 (EHL) to 0.132 over MoS_2 and further decreased to 0.129 over Ts-$W_{0.1}$@MoS_2 (Table 2). The lower O/C ratio signified that the catalytic DMO abilities were improved to promote more A-Ps formation. Therefore, W gave the highest promotion effect on MoS_2 because of the highest contents of Mo^{5+} in Ts-$W_{0.1}$@MoS_2 (32.1%, Figure 3), which led to the lowest O/C ratio in products.

3.4. Stability Analysis. Figure 8 shows the reusability of the Ts-$W_{0.1}$@MoS_2 and MoS_2 catalysts on the EHL depolymerization in ethanol. The yield of overall aromatic monomers and A-Ps were decreased on both undoped and W-

https://doi.org/10.1021/cbe.3c00062
Chem Bio Eng. 2024, 1, 725−736

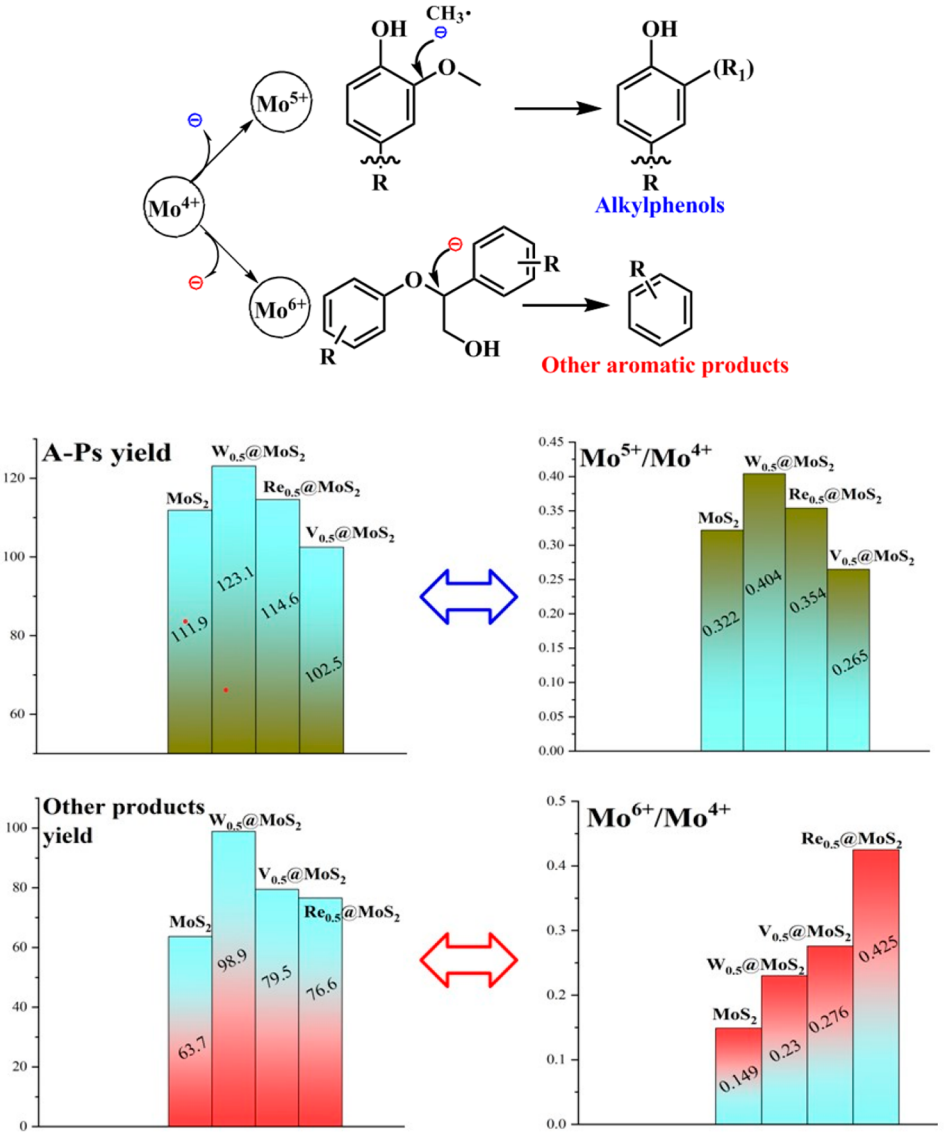

Figure 7. Effect of active metal doping on Mo-based sites of MoS_2 for each category of product from EHL ethanolysis.

Table 2. Atomic Ratio (H/C and O/C) and Heating Value of Liquid Products Obtained from EHL Depolymerization in Ethanol over Different Catalysts

Catalyst	O/C atomic ratio	H/C atomic ratio	Heating value/(MJ/kg)
MoS_2	0.132	1.432	35.8
Os-$W_{0.125}$@MoS_2	0.138	1.406	36.3
Ts-$W_{0.1}$@MoS_2	0.129	1.465	37.1

doped catalysts in the reusability studies. Specifically, when MoS_2 is used as the catalyst, the yields of overall aromatic monomers and A-Ps are decreased by 24.1% and 22.3%, respectively, after being used for 5 runs. However, the two values are decreased by 13.7% and 14.8%, respectively, when Ts-$W_{0.1}$@MoS_2 was used as the catalyst. The results indicate that the W-doping effectively improves the stability of MoS_2 during the recyclability test. Otherwise, the yields of overall aromatic monomers and A-Ps obtained over Ts-$W_{0.1}$@MoS_2 in the 5th run were 199.4 and 107.8 mg/g EHL, respectively, which are still at a higher yield level as compared to the fresh undoped MoS_2. Therefore, the W-doping effect significantly promotes the activity and stability of MoS_2 samples for EHL depolymerization to obtain aromatic monomers in the recyclability studies.

In our previous work, sulfur loss led to severe deactivation of MoS_2 on the demethoxylation of guaiacol in methanol.[29] Badawi et al.[28] also reported that the removal of surface sulfur atoms on the MoS_2 edge with oxygen atoms occurred, which was caused by the formation of water in the HDO of oxygenated compounds. The sulfur−oxygen exchange also led to continuous deactivation of the catalyst. Herein, the loss of atomic sulfur during the cycle experiments was discussed based on the XPS results shown in Table 3. The sulfur contents on MoS_2 and Ts-$W_{0.1}$@MoS_2 were decreased to 60.2% (from 75.9%) and 68.3% (from 72.3%), respectively, after 5 runs. Therefore, W-doping effectively improves the anti-sulfur loss ability of MoS_2 sample, which is significant to enhance the stability of the sample. Moreover, appropriate oxidation on the MoS_2 surface was beneficial to the EHL depolymerization as mentioned above, which has important influence on the

https://doi.org/10.1021/cbe.3c00062
Chem Bio Eng. 2024, 1, 725−736

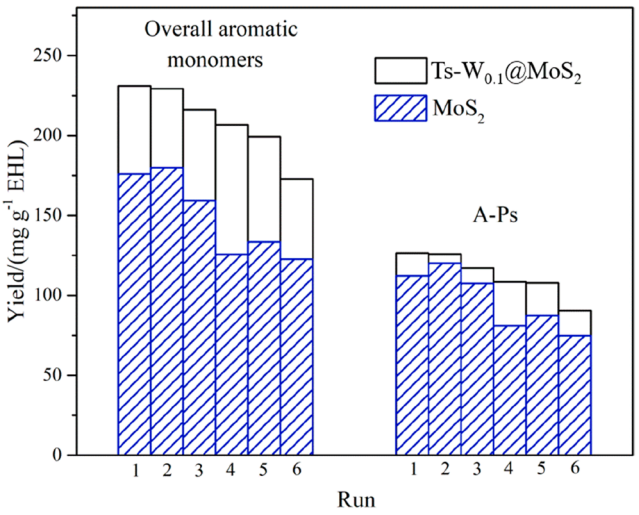

Figure 8. Recyclability of the Ts-$W_{0.1}$@MoS_2 and undoped MoS_2 catalysts on the yields of overall aromatic monomers and A-Ps obtained from the EHL depolymerization (reaction conditions: 1.0 g of EHL, 80 mL of ethanol, 0.5 g of catalyst, 320 °C, 6 h, initial 0 MPa (gauge) N_2, 600 rpm).

Table 3. Comparison of Undoped MoS_2 and Ts-$W_{0.1}$@MoS_2 (Fresh and Used after 5 Runs) Based on the XPS Analysis

		Undoped MoS_2		Ts-$W_{0.1}$@MoS_2	
		Fresh	Used after 5 runs	Fresh	Used after 5 runs
Atomic/%[a]	Mo	24.1	38.7	27.7	31.7
	S	75.9	61.3	72.3	68.3
Contents of Mo-based sites/%[b]	Mo^{4+}	68	32.3	52.4	49.1
	Mo^{5+}	21.9	27	32.1	17.8
	Mo^{6+}	10.1	40.7	15.6	33.1
$(Mo^{6+} + Mo^{5+})/Mo^{4+}$ [b]		0.471	2.096	0.908	1.037

[a]Relatively atomic contents of Mo and S on the surface of MoS_2 and Ts-$W_{0.1}$@MoS_2 based on the XPS analysis. Note: Only Mo and S are semiquantitative and the total content of Mo and S for each sample rounds to 100%. [b]XPS data of different Mo-based sites according to the results in Figure 3. The XPS analysis of undoped MoS_2 was not illustrated in Figure 3.

stability of the catalyst. The oxidation process of Mo-based sites on MoS_2 could be considered as the oxidation of Mo^{4+} into Mo^{5+} and Mo^{6+}. The ratio of $(Mo^{5+} + Mo^{6+})/Mo^{4+}$ can effectively measure the oxidation degree of the catalyst surface.[45] As listed in Table 3, the $(Mo^{5+} + Mo^{6+})/Mo^{4+}$ ratio of undoped MoS_2 was increased sharply from 0.471 to 2.096, which indicates that severe oxidation occurred in the recyclability studies. Nevertheless, W-doping modification leads to no significant change of the $(Mo^{5+} + Mo^{6+})/Mo^{4+}$ ratio for Ts-$W_{0.1}$@MoS_2, which was slightly increased from 0.908 to 1.037 after 5 runs use. Therefore, W-doping modification also improved the antioxidant ability of the catalyst, and the stability was also enhanced.

3.5. Proposal of W-Doping Effect. In order to understand the distribution of W atoms on MoS_2, the W/Mo atomic ratio of Ts-$W_{0.5}$@MoS_2, Ts-$W_{0.167}$@MoS_2, and Ts-$W_{0.1}$@MoS_2 are detected by XPS, XRF, and ICP, which presents the distribution of W atoms on the surface, near-surface, and bulk of MoS_2 (Figure 9).[27] The W/Mo atomic ratio is in the range $(15.1-16.0) \times 10^{-2}$ and $(1.57-3.61) \times 10^{-2}$ from XPS and XRF, respectively, which are much higher than that from ICP analysis ($\sim(0.580-1.50) \times 10^{-2}$). The results demonstrate that W atoms in W-doped MoS_2 samples are mainly distributed on the MoS_2 surface. Combined with the STEM-EDX analysis (Figure 2(b)) of Ts-$W_{0.1}$@MoS_2, tungsten atoms were proved to be well incorporated with MoS_2 surface.[27] In more detail, the W/Mo atomic ratio shows a decreasing trend by each while the W content is decreased in two-step hydrothermal samples. As for one-step hydrothermal samples, the Os-$W_{0.125}$@MoS_2 with higher W contents exhibits a three times higher W/Mo ratio (4.72×10^{-2}) than that of Ts-$W_{0.5}$@MoS_2 (1.57×10^{-2}), as shown in Table S1. These results reveal that the two-step hydrothermal method significantly promoted the distribution of more W atoms on the MoS_2 surface as compared to the one-step hydrothermal method.

Bai et al.[38] previously obtained the SEM images of the same EHL material used in this work. The average particle size of EHL was approximately in the range 20−80 μm. Nevertheless, the pore diameter of the studied catalysts is nanoscale, as shown in Table 1, which indicates the EHL sample is not penetrated into the pore of the catalyst, and the surface adsorption reaction cannot be realized. Ma et al.[46] proposed the detailed pathway of the product formation from Kraft lignin depolymerization in ethanol and supposed that lignin was first converted into lignin fragments via a noncatalytic ethanolysis process. The lignin fragments were regarded as the reactant on the catalyst to achieve the surface adsorption reaction. Subsequently, the 2D-HSQC NMR of the liquid

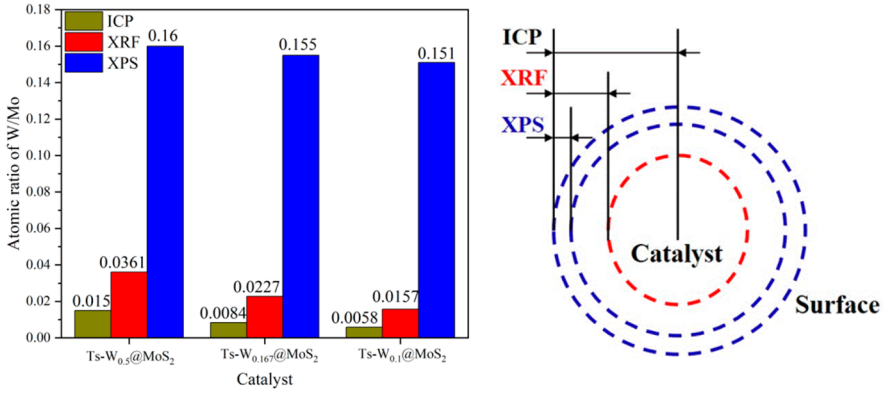

Figure 9. W/Mo atomic ratio of Ts-$W_{0.5}$@MoS_2, Ts-$W_{0.1}$@MoS_2, and Os-$W_{0.125}$@MoS_2 catalysts detected by ICP, XRF, and XPS.

https://doi.org/10.1021/cbe.3c00062
Chem Bio Eng. 2024, 1, 725−736

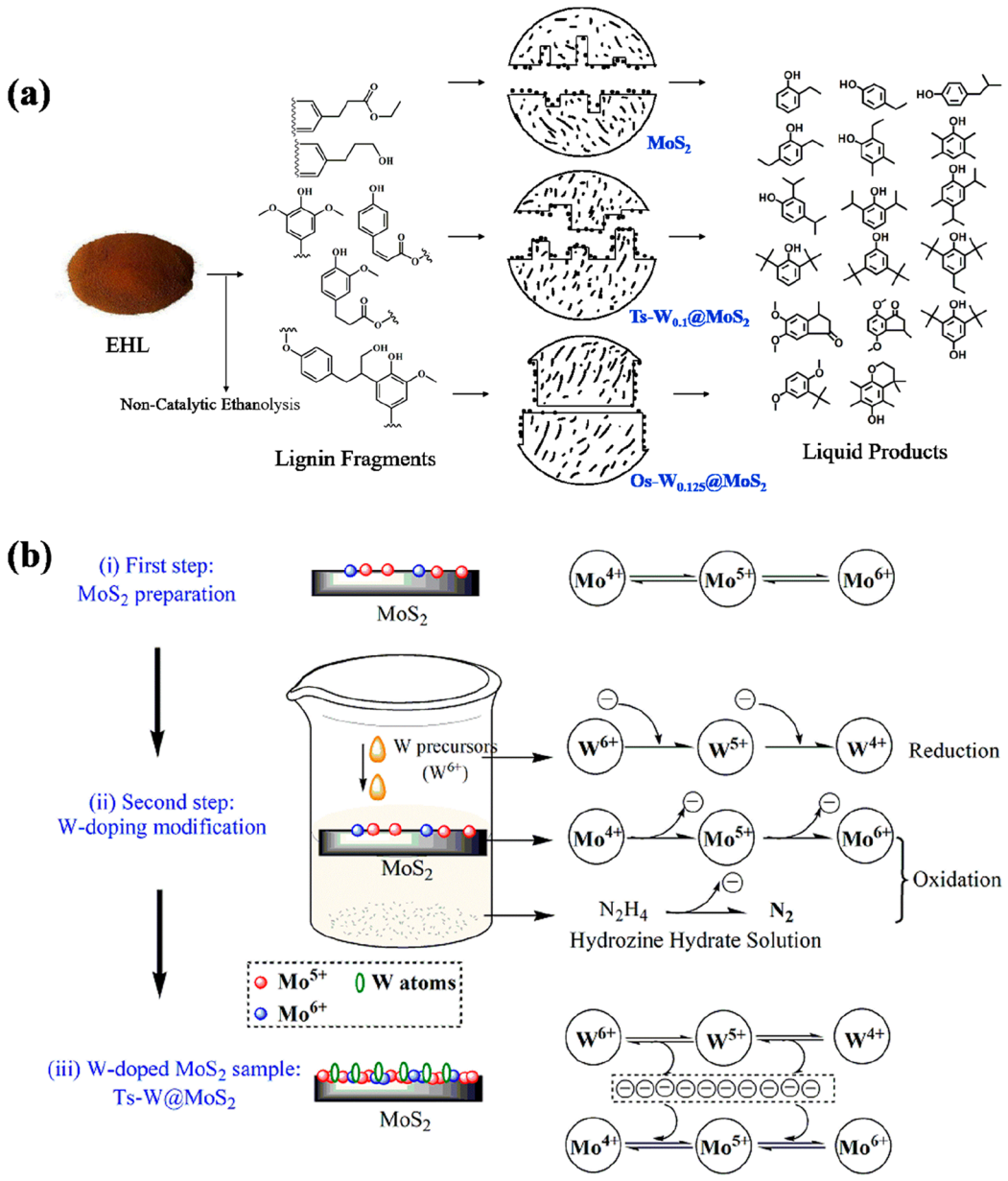

Figure 10. (a) Proposal of the pathway of EHL depolymerization into liquid products over MoS_2, Ts-$W_{0.1}$@MoS_2, and Os-$W_{0.125}$@MoS_2 samples and the effect of W-doping on the conversion pathway. (b) Proposal of the effect of W-doping on MoS_2 during the two-step hydrothermal preparation process.

products from EHL ethanolysis without catalyst is further operated as shown in Table S2. The signals of $-CH_3$, methoxy groups, *para*-methyl aromatic groups (PM), *para*-ethyl aromatic groups (PE), *para*-propyl aromatic groups (PP), *para*-syringyl units of lignin (S), *p*-coumaric acid (CA), ferulic acid derivatives (HFA), and a dimer-containing structure (A) were detected in the post-reaction liquid without catalyst. Therefore, the pathway of the depolymerization was proposed, as shown in Figure 10(a). EHL first underwent a noncatalytic ethanolysis process to form the liquid products, which contains the above-mentioned structural units. These lignin fragments are further penetrated into the pore of the catalyst. To clearly understand the W-doping effect on MoS_2, the catalyst models of MoS_2, Ts-$W_{0.1}$@MoS_2, and Os-$W_{0.125}$@MoS_2 are supposed to be based on the texture data in Table 1. The pore diameter of W-doped MoS_2 is significantly increased compared to that of undoped MoS_2, which promotes the lignin fragments to easily access the catalyst pore and realize the surface adsorption reaction. Meanwhile, the increased special surface area for Ts-$W_{0.1}$@MoS_2 allows more catalyst active sites to be exposed and further co-reacted with lignin fragments.

Valencia et al.[47] discussed that the content of Mo^{6+}, Mo^{5+}, and Mo^{4+} in the Mo-based catalyst played a significant role on the activity of palmitic acid HDO reaction. A catalytic cycle among the different active sites was proposed to comprehend the influence of the catalyst on the HDO reaction. Herein, the similar catalytic cycle among Mo^{6+}, Mo^{5+}, and Mo^{4+} can also be proposed in the MoS_2 plane, as shown in Figure 10(b(i)). In the second step of W-doping modification, W precursors (W^{6+}) are added into the undoped MoS_2-containing hydrazine hydrate solution. Based on the XPS results of W-doped samples (Figure 3(c)), W^{5+} is the most important species on

https://doi.org/10.1021/cbe.3c00062
Chem Bio Eng. 2024, 1, 725−736

the MoS_2 surface, which indicates the W precursor occurs in the reduction reaction on MoS_2 (Figure 10(b(ii)). Moreover, after W-doping modification, the contents of Mo^{5+} and Mo^{6+} on undoped MoS_2 are increased to 32.1% (from 21.9%) and 15.6% (from 10.1%), respectively, on Ts-$W_{0.1}$@MoS_2, and 27.2% and 22.6%, respectively, on Os-$W_{0.125}$@MoS_2. These results imply that Mo-based sites also occur in oxidation reactions during the W-doping process. Meanwhile, hydrazine could be easily oxidized into nitrogen. Therefore, the effect of W-doping modification is mainly embodied in the reduction of W precursors on MoS_2via capturing the free electrons, which promotes the oxidation of Mo^{4+} and hydrazine to release the free electrons. More active Mo^{5+} and Mo^{6+} sites on MoS_2 are generated with the effect of W-doping as shown in Figure 10(b(iii)). In addition, the severe oxidation reaction among Mo-based sites results in the deactivation of MoS_2, which might be due to damage of the catalytic cycles among different Mo-based sites (Figure 10(b, (i)). While W is doped on MoS_2 (Ts-$W_{0.1}$@MoS_2), the W^{4+} and W^{5+} are decreased into 5.5% and 48.2%, respectively, after being used for 5 runs, as shown in Figure 3(c). On the consideration of the well incorporation of W atoms with the MoS_2 surface, the effect of the W-doping on the stability of MoS_2 is further proposed as shown in Figure 10(b,(iii)). In the recyclability test, W^{4+} and W^{5+} are significant oxidation reactions, and more electrons are released, which promotes the reduction reaction of Mo-based sites. The balance of catalytic cycles among different Mo-based sites was significantly improved, which contributed to the enhancement of MoS_2 after W-doping modification.

4. CONCLUSION

A series of active metals (Re, V, and W) were doped on MoS_2 synthesized via a two-step hydrothermal method for the activity investigation of EHL depolymerization in ethanol. The highest yield of overall aromatic monomers and alkylphenols (A-Ps) of 231 and 126.5 mg/g EHL, respectively, were achieved over Ts-$W_{0.1}$@MoS_2 at 320 °C, which gave higher improvement of bio-oils' heating value (37.1 MJ/kg). Two-step hydrothermal synthesized samples exhibited much higher activity than one-step prepared ones on the higher achievements of overall aromatic monomers, which were ascribed to large specific area and homogeneous distribution of W atoms on MoS_2 surface. The Mo^{5+}/Mo^{4+} value on MoS_2 was effectively increased by doping W (or Re), which promoted the yield enhancement of alkylphenols from EHL depolymerization. The W-doping modification significantly improved activity and stability (including anti-sulfur loss and antioxidant abilities) of the MoS_2 samples in the recyclability test. Good incorporation of the W atoms with the MoS_2 surface and the oxidation of W-based sites in the recyclability test promote the balance of catalytic cycles among different Mo-based sites on MoS_2 surface, which leads to the enhancement of stability for W-doped MoS_2 samples.

ASSOCIATED CONTENT

Supporting Information

The Supporting Information is available free of charge at https://pubs.acs.org/doi/10.1021/cbe.3c00062.

N_2 adsorption−desorption isotherms, XPS of different samples, and tables of W/Mo atomic ratios and signal assignments 2D-HSQC of noncatalytic obtained liquids (PDF)

AUTHOR INFORMATION

Corresponding Author

Jianming Yang − *Xi'an Modern Chemistry Research Institute, Xi'an, Shaanxi 710065, China; State Key Laboratory of Fluorine & Nitrogen Chemicals, Xi'an, Shaanxi 710065, China;* orcid.org/0000-0001-5177-9649; Email: yangjm204@163.com

Authors

Kai Wu − *Xi'an Modern Chemistry Research Institute, Xi'an, Shaanxi 710065, China; State Key Laboratory of Fluorine & Nitrogen Chemicals, Xi'an, Shaanxi 710065, China*

Qian Zhang − *Xi'an Modern Chemistry Research Institute, Xi'an, Shaanxi 710065, China*

Yuanbo Zheng − *Xi'an Modern Chemistry Research Institute, Xi'an, Shaanxi 710065, China*

Jun Yuan − *Xi'an Modern Chemistry Research Institute, Xi'an, Shaanxi 710065, China*

Qinwei Yu − *Xi'an Modern Chemistry Research Institute, Xi'an, Shaanxi 710065, China; State Key Laboratory of Fluorine & Nitrogen Chemicals, Xi'an, Shaanxi 710065, China*

Jian Lu − *Xi'an Modern Chemistry Research Institute, Xi'an, Shaanxi 710065, China; State Key Laboratory of Fluorine & Nitrogen Chemicals, Xi'an, Shaanxi 710065, China;* orcid.org/0000-0002-0494-2498

Complete contact information is available at: https://pubs.acs.org/10.1021/cbe.3c00062

Author Contributions

Kai Wu: Methodology, Investigation, Writing−original draft. Qian Zhang: Writing−review & editing. Yuanbo Zheng: Formal analysis. Jun Yuan: Formal analysis. Qinwei Yu: Validation. Jianming Yang: Supervision, Conceptualization, Writing - review & editing. Jian Lu: Supervision, Conceptualization, Funding acquisition.

Notes

The authors declare no competing financial interest.

ACKNOWLEDGMENTS

We acknowledge financial support from National Natural Science Foundation of China (Grant Nos.: 21902124, 22072112) and Key Research and Development Projects of Shanxi Province (Grant Nos.: M-ZX-JT-2201T, M-ZX-JT-2202T04, M-ZX-JT-2202T05, 2023-YBGY-176).

REFERENCES

(1) Han, Y. L.; Simmons, B. A.; Singh, S. Perspective on oligomeric products from lignin depolymerization: their generation, identification, and further valorization. *Ind. Chem. Mater.* **2023**, *1*, 207.

(2) Liao, Y. H.; Koelewijn, S. F.; Bossche, G. V. D.; Aelst, J. V.; Bosch, S. V. D.; Renders, T.; Navare, K.; Nicolai, T.; Aelst, K. V.; Maesen, M.; Matsushima, H.; Thevelein, J. M.; Acker, K. V.; Lagrain, B.; Verboekend, D.; Sels, B. F. A sustainable wood biorefinery for low-carbon footprint chemicals production. *Science* **2020**, *367*, 1385−1390.

(3) Chantranupong, L.; Ceron, C. C.; Zimmer, J. A.; Wen, M. J.; Wang, W. G.; Sabatini, B. L. Dopamine and glutamate regulate striatal acetylcholine in decision-making. *Nature* **2023**, *621*, 577−585.

(4) Su, S. H.; Cao, F. S.; Wang, S. Z.; Shen, Q. R.; Luo, G.; Lu, Q.; Song, G. Y. Organoborane-catalysed reductive depolymerisation of catechyl lignin under ambient conditions. *Green Chem.* **2023**, *25*, 8172−8180.

(5) Gao, J. Q.; Yu, W.; Li, Y. X.; Jin, M. J.; Yao, L.; Zhou, Y. J. Engineering co-utilization of glucose and xylose for chemical overproduction from lignocelluloses. *Nature Chem. Bio.* **2023**, *19*, 1524−1531.
(6) Ma, J.; Le, D.; Yan, N. Single-step conversion of wood lignin into phenolic amines. *Chem.* **2023**, *9*, 2869−2880.
(7) Agarwal, A.; Rana, M.; Park, J. H. Advancement in technologies for the depolymerization of lignin. *Fuel Process. Technol.* **2018**, *181*, 115−131.
(8) Figueiredo, M. B.; Keij, F. W.; Hommes, A.; Deuss, P. J.; Venderbosch, R. H.; Yue, J.; Heeres, H. J. Efficient depolymerization of lignin to biobased chemicals using a two-step approach involving ozonation in a continuous flow microreactor followed by catalytic hydrotreatment. *ACS Sustain. Chem. Eng.* **2019**, *7*, 18384−19394.
(9) Li, J.; Galebach, P. H.; Johnson, J. K.; Fredriksen, T.; Wittrig, A.; Bai, X. W.; Yang, H. P.; Huber, G. W. Supercritical methanol depolymerization and hydrodeoxygenation of pyrolytic lignin over reduced copper porous metal oxides. *ACS Sustainable Chem. Eng.* **2020**, *22*, 8403−8413.
(10) Liu, Q. F.; Bai, Y. F.; Chen, H.; Chen, M. M.; Sang, Y. S.; Wu, K.; Ma, Z. W.; Ma, Y. M.; Li, Y. D. Catalytic conversion of enzymatic hydrolysis lignin into cycloalkanes over a gamma-alumina supported nickel molybdenum alloy catalyst. *Bioresource Technol.* **2021**, *323*, 124634−124639.
(11) Gao, D. H.; Quyang, D. H.; Zhao, X. B. Electro-oxdative depolymerization of lignin for production of value-added chemicals. *Green Chem.* **2022**, *24*, 8585−8605.
(12) Meng, T. T.; Ding, Y.; Liu, Y.; Xu, L.; Mao, Y. M.; Gelfond, J. L.; Li, S. K.; Li, Z. H.; Salipante, P. F.; Kim, H.; Zhu, J. Y.; Pan, X. J.; Hu, L. B. In Situ adhesion for high-performance bamboo composites. *Nano Lett.* **2023**, *23*, 8411−8418.
(13) Sirous Rezaei, P.; Jae, J.; Ha, J. M.; Ko, C. H.; Kim, J. M.; Jeon, J. K.; Park, Y. K. Mild hydrodeoxygenation of phenolic lignin model compounds over a $FeReO_x$ /ZrO_2 catalyst: Zirconia and rhenium oxide as efficient dehydration promoters. *Green Chem.* **2018**, *20*, 1472−1483.
(14) Bau, J. A.; Emwas, A. H.; Nikolaienko, P.; Aljarb, A. A.; Ting, V.; Rueping, M. Mo^{3+} hydride as the commonorigin of H_2 evolution and selective NADH regeneration in molybdenum sulfide electrocatalysts. *Nat. Catal.* **2022**, *5*, 397−404.
(15) Liu, J. P.; Liu, Y. Z.; Xu, D.Y.; Zhu, Y. Z.; Peng, W. C.; Li, Y.; Zhang, F. B.; Fan, X. B. Hierarchical "nanroll" like $MoS_2/Ti_3C_2T_x$ hybrid with high electrocatalytic hydrogen evolution activity. *Appl. Catal., B* **2019**, *241*, 89−94.
(16) Shabtai, J.; Nag, N. K.; Massoth, F. E. Catalytic functionalities of supported sulfides: IV. C-O hydrogenolysis selectivity as a function of promoter type. *J. Catal.* **1987**, *104*, 413−423.
(17) Wang, Z. F.; Kang, Y. R.; Hu, J. T.; Ji, Q. Q.; Lu, Z. X.; Xu, G. L.; Qi, Y. T.; Zhang, M.; Zhang, W. W.; Huang, R.; Yu, L.; Tian, Z. Q.; Deng, D. H. Boosting CO_2 hydrogenation to formate over edge-sulfur vacancies of molybdenum disulfide. *Angew. Chem. Int. Ed.* **2023**, *62*, 45.
(18) Bui, V. N.; Laurenti, D.; Afanasiev, P.; Geantet, C. Hydrodeoxygenation of guaiacol with CoMo catalysts. Part I: Promoting effect of cobalt on HDO selectivity and activity. *Appl. Catal., B* **2011**, *101*, 239−245.
(19) Shi, Z. Y.; Zhang, X.; Lin, X. Q.; Liu, G. G.; Ling, C. Y.; Xi, S. B.; Chen, B.; Ge, Y. Y.; Tan, C. L.; Lai, Z. C.; Huang, Z. Q.; Ruan, X. Y.; Zhai, L.; Li, L. J.; Li, Z. J.; Wang, X. X.; Nam, G. H.; Liu, J. W.; He, Q. Y.; Guan, Z. Q.; Wang, J. L.; Lee, C. S.; Kucernak, A. R. J.; Zhang, H. Phase-dependent growth of Pt on MoS_2 for highly efficient H_2 evolution. *Nature* **2023**, *621*, 300−305.
(20) Karunadasa, H. I.; Montalvo, E.; Sun, Y.; Majda, M.; Long, J. R.; Chang, C. J. A molecular MoS_2 edge site mimic for catalytic hydrogen generation. *Science* **2012**, *335*, 698−702.
(21) Liu, A.; Zhao, L.; Zhang, J.; Liu, L.; Wu, H. Solvent-assisted oxygen incorporation of vertically aligned MoS_2 ultrathin nano-sheets decorated on reduced graphene oxide for improved electrocatalytic hydrogen evolution. *ACS Appl. Mater. Interfaces* **2016**, *8*, 25210−25218.
(22) Luo, Z. Y.; Zhang, H.; Yang, Y. Q.; Wang, X.; Li, Y.; Jin, Z.; Jiang, Z.; Liu, C. P.; Xing, W.; Ge, J. J. Reactant friendly hydrogen evolution interface based on di-anionic MoS_2 surface. *Nat. Commun.* **2020**, *11*, 1116.
(23) Leyral, G.; Brillouet, S.; Rousseau, J.; Richard, F.; Mamede, A. S.; Courthéoux, L.; Pradel, A.; Ribes, M.; Brunet, S. Effect of the presence of ionic liquid during the NiMoS bulk preparation in the transformation of decanoic acid. *Appl. Catal. A-Gen.* **2017**, *532*, 120−132.
(24) Shi, Y.; Zhou, Y.; Yang, D. R.; Xu, W. X.; Wang, C.; Wang, F. B.; Xu, J. J.; Xia, X. H.; Chen, H. Y. Energy level engineering of MoS_2 by transition-metal doping for accelerating hydrogen evolution reaction. *J. Am. Chem. Soc.* **2017**, *139*, 15479−15485.
(25) Wu, Z. X.; Guo, J. P.; Wang, J.; Liu, R.; Xiao, W. P.; Xuan, C. J.; Xia, K. D.; Wang, D. L. Hierarchically porous electrocatalyst with vertically aligned defect-rich CoMoS nanosheets for the hydrogen evolution reaction in an alkaline medium. *ACS Appl. Mater. Interfaces* **2017**, *9*, 5288−5294.
(26) Wang, W. Y.; Li, L.; Wu, K.; Zhu, G. H.; Tan, S.; Liu, Y.; Yang, Y. Q. Highly selective catalytic conversion of phenols to aromatic hydrocarbons on CoS_2/MoS_2 synthesized using a two-step hydrothermal method. *RSC Adv.* **2016**, *6*, 31265−31271.
(27) Song, W. J.; Zhou, S. J.; Hu, S. H.; Lai, W. K.; Lian, Y. X.; Wang, J. Q.; Yang, W. M.; Wang, M. Y.; Wang, P.; Jiang, X. M. Surface engineering of CoMoS nanosulfide for hydrodeoxygenation of lignin-derived phenols to arenes. *ACS Catal.* **2019**, *9*, 259−268.
(28) Badawi, M.; Cristol, S.; Paul, J.; Payen, E. DFT study of furan adsorption over stable molybdenum sulfide catalyst under HDO conditions. *CR. Chim.* **2009**, *12*, 754−761.
(29) Wu, K.; Kasipandi, S.; Wen, Z.; Yan, F.; Sang, Y. S.; Ma, Z. W.; Chen, M. M.; Chen, H.; Li, Y. D. Selective demethoxylation of guaiacol to alkylphenols in supercritical methanol over a HT-MoS_2 catalyst. *Catal. Today* **2021**, *368*, 260−271.
(30) Delporte, P.; Meunier, F.; Pham-Huu, C.; Vennegues, P.; Ledoux, M. J.; Guille, J. Physical characterization of molybdenum oxycarbide catalyst; TEM, XRD and XPS. *Catal. Today* **1995**, *23*, 251−267.
(31) Katrib, A.; Benadda, A.; Sobczak, J. W.; Maire, G. XPS and catalytic properties of the bifunctional supported MoO_2(Hx)ac on TiO_2 for the hydroisomerization reactions of hexanes and 1-hexene. *Appl. Catal. A-Gen.* **2003**, *242*, 31−40.
(32) Yu, H.; Zhu, C.; Zhang, K.; Chen, Y.; Li, C.; Gao, P.; Yang, P.; Quyang, Q. Three-dimensional hierarchical MoS_2 nanoflake array/carbon cloth as high-performance flexible lithium-ion battery anodes. *J. Mater. Chem. A* **2014**, *2*, 4551−4557.
(33) Diao, X. Y.; Ji, N.; Zheng, M. Y.; Liu, Q. L.; Song, C. F.; Huang, Y. B.; Zhang, Q.; Alemayehu, A.; Zhang, L. Y.; Liang, C. H. MgFe hydrotalcites-derived layered structure iron molybdenum sulfide catalysts for eugenol hydrodeoxygenation to produce phenolic chemicals. *J. Energy Chem.* **2018**, *27*, 600−610.
(34) Ji, N.; Diao, X. Y.; Li, X. X.; Jia, Z. C.; Zhao, Y. J.; Lu, X. B.; Song, C. F.; Liu, Q. L.; Li, C. Z. Toward alkylphenols production: Lignin depolymerization coupling with methoxy removal over supported MoS_2 catalyst. *Ind. Eng. Chem. Res.* **2020**, *59*, 17287−17299.
(35) Echeandia, S.; Arias, P. L.; Barrio, V. L.; Pawelec, B.; Fierro, J. L. G. Synergy effect in the HDO of phenol over Ni-W catalysts supported on active carbon: Effect of tungsten precursors. *Appl. Catal., B* **2010**, *101*, 1−12.
(36) Mallesham, B.; Sudarsanam, P.; Raju, G.; Reddy, B. M. Design of highly efficient Mo and W-promoted SnO_2 solid acids for heterogeneous catalysis: acetalization of bio-glycerol. *Green Chem.* **2013**, *15*, 478−489.
(37) Tayebi, M.; Masoumi, Z.; Lee, B. Ultrasonically prepared photocatalyst of W/WO_3 nanoplates with WS_2 nanosheets as 2D material for improving photoelectrochemical water splitting. *Ultrason. Sonochem.* **2021**, *70*, 105339.

https://doi.org/10.1021/cbe.3c00062
Chem Bio Eng. 2024, 1, 725−736

(38) Bai, Y. F.; Cui, K.; Sang, Y. S.; Wu, K.; Yan, F.; Mai, F. H.; Ma, Z. W.; Wen, Z.; Chen, H.; Li, Y. D.; Chen, M. M. Catalytic depolymerization of a lignin-rich corncob residue into aromatics in supercritical ethanol over an alumina-supported NiMo alloy catalyst. *Energy Fuels* **2019**, *33*, 8657−8665.
(39) Romero, Y.; Richard, E.; Brunet, S. Hydrodeoxygenation of 2-ethylphenol as a model compound of bio-crude over sulfided Mo-based catalysts: Promoting effect and reaction mechanism. *Appl. Catal., B* **2010**, *98*, 213−223.
(40) Topsøe, N.-Y.; Topsøe, H. Characterization of the structures and active sites in sulfided Co-$MoAl_2O_3$ and Ni-$MoAl_2O_3$ catalysts by NO chemisorption. *J. Catal.* **1983**, *84*, 386−401.
(41) Topsøe, H.; Clausen, B. S. Importance of Co-Mo-S type structures in hydrodesulfurization. *Catal. Rev.* **1984**, *26*, 395−420.
(42) Lauritsen, J. V.; Kibsgaard, J.; Olesen, G. H.; Moses, P. G.; Hinnemann, B.; Helveg, S.; Nørskov, J. K.; Clausen, B. S.; Topsøe, H.; Lægsgaard, E.; Besenbacher, F. Location and coordination of promoter atoms in Co- and Ni-promoted MoS_2-based hydrotreating catalysts. *J. Catal.* **2007**, *249*, 220−233.
(43) Luo, W.; Shi, H.; Schachtl, E.; Gutiérrez, O.; Lercher, J. Active sites on nickel-promoted transition-metal sulfides that catalyze hydrogenation of aromatic compounds. *Angew. Chem. Int. Ed.* **2018**, *57*, 14555−14559.
(44) Cui, K.; Yang, L.; Ma, Z. W.; Yan, F.; Wu, K.; Sang, Y. S.; Chen, H.; Li, Y. D. Selective conversion of guaiacol to substituted alkylphenols in supercritical ethanol over MoO_3. *Appl. Catal., B* **2017**, *219*, 592−602.
(45) Wu, K.; Sang, Y. S.; Kasipandi, S.; Ma, Y. M.; Jiao, H. R.; Liu, Q. F.; Chen, H.; Li, Y. D. Catalytic roles of Mo-based sites on MoS_2 for ethanolysis of enzymatic hydrolysis lignin into aromatic monomers. *Catal. Today* **2023**, *408*, 211−222.
(46) Ma, X. L.; Ma, R.; Hao, W. Y.; Chen, M. M.; Yan, F.; Cui, K.; Li, Y. D. Common pathways in ethanolysis of Kraft lignin to platform chemicals over molybdenum-based catalysts. *ACS Catal.* **2015**, *5*, 4803−4813.
(47) Valencia, D.; Díaz-García, L.; Ramírez-Verduzco, L. F.; Qamar, A.; Moewes, A.; Aburto, J. Paving the way towards green catalytic materials for green fuels: impact of chemical species on Mo-based catalysts for hydrodeoxygenation. *RSC Adv.* **2019**, *9*, 18292−18301.

https://doi.org/10.1021/cbe.3c00062
Chem Bio Eng. 2024, 1, 725−736